High Selectivity Reactive Carbon Dioxide Capture over Zeolite Dual-Functional Materials

AUTHORS

James M. Crawford[†,], Mathew J. Rasmussen[‡], W. Wilson McNeary[‡], Sawyer Halingstad[‡], Steven C. Hayden[Ω], Nikita S. Dutta[Ω], Simon H. Pang[Ψ], Matthew M. Yung[‡,*]*

ADDRESSES

[†]Department of Chemical & Biological Engineering, Montana State University, 214 Roberts Hall, Bozeman, MT 59717

[‡]Bioenergy Science and Technology Directorate, National Renewable Energy Laboratory, 15013 Denver West Parkway, Golden, CO 80401

[Ω]Materials, Chemical, and Computational Science Directorate, National Renewable Energy Laboratory, 15013 Denver West Parkway, Golden, CO 80401

[Ψ]Materials Science Division, Lawrence Livermore National Laboratory, Livermore, CA 94550

GRAPHICAL ABSTRACT

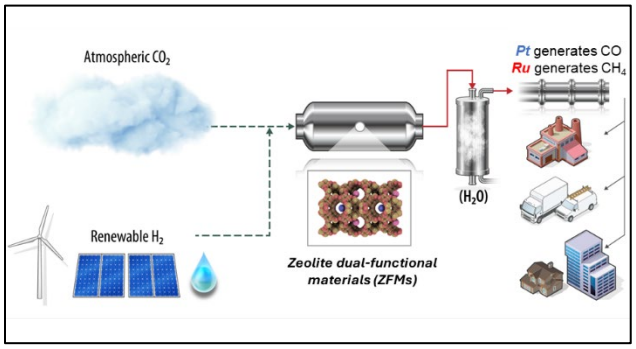

3.25 x 1.75

ABSTRACT

Reactive carbon capture (RCC) is a process where carbon dioxide (CO_2) is captured from a mixed gas stream (such as air) and converted to products without first performing a separation step to concentrate CO_2. In this work, zeolite dual-functional materials (ZFMs) are introduced and evaluated for simulated RCC. The studied ZFMs feature high surface area, crystalline, microporous zeolite faujasite (FAU) as the support. Sodium oxide ("Na_2O") is impregnated as an effective capture agent capable of scavenging low concentration CO_2 (1,000 ppm). Exchanged and impregnated sodium on FAU chemisorbs CO_2 as carbonates and bicarbonates but does not promote the conversion of sorbed CO_2 to products when heated in hydrogen. The addition of Ru promotes the formation of formates while the addition of Pt generates carbonyl surface species when heated in hydrogen. The active metal then promotes extremely high selectivity for CO_2 hydrogenation to either methane on Ru catalyst (~150 °C) or carbon monoxide on Pt catalyst (~200 °C) when heated in reducing atmospheres.

KEYWORDS

Carbon dioxide utilization, reactive carbon capture, zeolite, ruthenium, platinum, hybrid sorbent-catalyst, methane, carbon monoxide, hydrogenation

MAIN TEXT

Roughly 36 billion tons of carbon dioxide (CO_2) are added annually to the current ~3.2 trillion ton atmospheric inventory[1]. Pending development of efficient capture and selective synthetic pathways, fuels and chemicals could be derived from atmospheric CO_2 and replace global reliance on underground resources such as oil and gas. Replacing petroleum-derived fuels with aboveground carbon resources is of vital importance to slow or reverse trends in global warming[2].

Significant attention has been given to building energy-efficient unit operations for CO_2 upgrading. Processing steps currently required for atmospheric CO_2 upgrading include: 1) CO_2 adsorption via direct air capture, 2) temperature/vacuum swing desorption, 3) compression, 4) pipeline/rail/truck transport of the compressed CO_2, and 5) conversion to products with co-fed hydrogen[3]. Combining the capture and conversion steps is of great interest for improved efficiency and simplified operation and would allow elimination of compression and transport. Process intensification also lowers the system footprint, which could increase global adoption of the technology. Thus, reactive carbon capture (RCC) has been proposed as a solution that combines the aforementioned processing steps into one unit[4]. Here, we focus on the selective hydrogenation of CO_2 to either CH_4 (Equation 1) or CO (Equation 2):

Equation 1: $CO_2 + 4 \cdot H_2 \rightarrow CH_4 + 2 \cdot H_2O$, Sabatier Reaction

Equation 2: $CO_2 + H_2 \rightarrow CO + H_2O$, Reverse water-gas shift

A class of hybrid sorbent-catalysts (HSCs) endowed with RCC capabilities, coined dual-functional materials (DFMs)[5,6], have been tailored to direct air capture[7,8] and point source emission capture applications[9,10]. One well studied DFM is Ru-Na/Al_2O_3. This material is capable of CO_2 collection from low concentration streams (via chemisorption on sodium oxides) and sequential conversion to CH_4 upon heating in hydrogen (via H_2 dissociation on Ru sites). Ru-Na/Al_2O_3 exhibits high selectivity for the methanation pathway while utilizing small quantities of precious metal. Significant work has been done to understand various important aspects of the Ru-Na/Al_2O_3 DFM including support, sorbent, active site, and cycling effects[11,12]. Areas of continuous improvement and optimization include material durability, catalyst cost, product purity, and simplified/energy-efficient RCC cycles. In the current work we introduce zeolite-based HSCs, termed zeolite dual-

functional materials (ZFMs), which are endowed with uniquely high CH_4 or CO selectivity depending on the active metal: either Ru or Pt, respectively.

Zeolites host cations at framework sites that can be modified by ion exchange treatments. Faujasite (FAU) is a large pore zeolite (limiting pore aperture of 7.35 Å) with three primary exchange sites (I/I' in the sodalite cage, II/II' in the hexagonal rings, and III/III' in the entrance of the supercage)[13]. Modifying the exchange sites changes the CO_2 adsorption properties of the zeolite. As previously demonstrated by LeVan and co-workers, smaller ionic radius monovalent cations increase the CO_2 capacity in low Si/Al FAU zeolites[14]. Thus, we selected a sodium-exchanged FAU zeolite (Si/Al = 1.5) as our support (Na-FAU). Hattori and coworkers showed that the addition of extra-framework Na (Na saturating exchange sites and also in extra-framework sites) promoted significantly higher CO_2 uptake in FAU zeolites compared to materials with Na present only in the exchange sites[15]. Thus, we added additional sodium to Na-FAU by impregnating sodium carbonate via incipient wetness to obtain a total sodium loading of ~20 %, giving our Na/FAU catalyst (catalyst compositions can be found in **Table S1**). The Na/FAU sample exhibited a reduced specific surface area and pore volume compared to Na-FAU as measured by N_2-physisorption (**Figure 1**A, **Table S1**). The loss of surface area (~68 % loss) and pore volume (~53 % loss), evidenced by the loss of uptake at low N_2 partial pressure, was greater than the dilution by addition of non-porous Na (~20 % loss anticipated) indicating that extra-framework sodium was either deposited within the micropores or blocked the micropores externally. To obtain the ZFMs we impregnated 1 wt.% Ru or 1 wt.% Pt on Na/FAU, yielding the Ru-Na/FAU or Pt-Na/FAU (**Table S2**). The addition of Ru or Pt to Na/FAU did not significantly influence the surface area or pore volume.

Hydrogen temperature programmed reduction (H_2-TPR) was conducted to evaluate the thermal requirements for reduction of the dispersed Ru or Pt (**Figure 1**B). During the RCC process, it is vital that the active metal sites begin to reduce before CO_2 desorption occurs, otherwise, CO_2 will desorb unreacted[9]. For H_2-TPR, catalysts were first oxidized in 10% O_2/He at 400 °C, cooled to 50 °C, then heated in 5% H_2/Ar to 300 °C. Ru-Na/FAU showed low and high temperature reduction peaks (T_{max} ~ 115, 250 °C, respectively). Pt-Na/FAU showed a low temperature shoulder (T_{max} ~ 175 °C) and a high temperature reduction peak (T_{max} ~ 240 °C). The two reduction steps could indicate a two-step reduction of metal dioxides (RuO_2 and PtO_2) or suggest heterogeneous metal speciation/varied support interactions. After reduction, metallic Pt phases were observed on Pt-Na/FAU via X-ray diffraction (XRD), but no additional reflections were observed on Ru-Na/FAU compared to the parent Na/FAU (**Figure 1**F).

To evaluate catalyst basicity, carbon dioxide temperature programmed desorption (CO_2-TPD) was conducted (Figure 1C). The anticipated effect of adding extra-framework Na to Na-FAU was observed[15], where CO_2 adsorption was enhanced on Na/FAU. Interestingly, the addition of Ru and Pt further enhanced the adsorption of CO_2; CO_2 chemisorption has been reported on platinum-group metals[8,16]. Importantly, on all samples, CO_2 desorption initiates just above 150 °C. From H_2-TPR, we have shown that Ru-Na/FAU begins to reduce at ~115 °C which is considerably lower than the CO_2 desorption temperature. The Pt-Na/FAU first reduces at ~175 °C, which is slightly above the initial CO_2 desorption feature.

Catalyst acidity was probed via ammonia temperature programmed desorption (NH_3-TPD, **Figure 1**D). The Na-FAU support had a low temperature desorption peak (T_{max} ~ 200 °C) and a high temperature shoulder (T_{max} ~ 325 °C). The addition of extra-framework sodium (Na/FAU) decreased the low temperature peak and entirely removed the high temperature NH_3 desorption

feature. The addition of Ru or Pt further decreased the low temperature NH_3 desorption feature. To evaluate the presence of Lewis and/or Brønsted acidity, catalysts were exposed to pyridine and examined using diffuse reflectance Fourier transform infrared spectroscopy (py-DRIFTS, **Figure 1**E). Na-FAU showed three pronounced features at 1441, 1488, and 1590 cm^{-1}. Ferwerda et al. found that Lewis acid sites, $Na^{\delta+}$ interacting with pyridine, generated spectral features at 1441 and 1590 cm^{-1} and that Lewis and/or Brønsted acidity could promote the observed feature at 1488 cm^{-1} for Na exchanged FAU[17]. Addition of extra-framework Na and Ru/Pt removed the feature at 1488 cm^{-1} and reduced the features at 1441 and 1590 cm^{-1}. Additional spectra were collected as samples were heated to 400 °C (**Figure S1**). Combining the findings from NH_3-TPD and py-DRIFTS, it was concluded that Lewis acid sites were the dominant acidic species on the Na/FAU, Ru-Na/FAU, and Pt-Na/FAU catalysts and that the addition of Na, Ru, and Pt decreased the total acidity compared to Na-FAU.

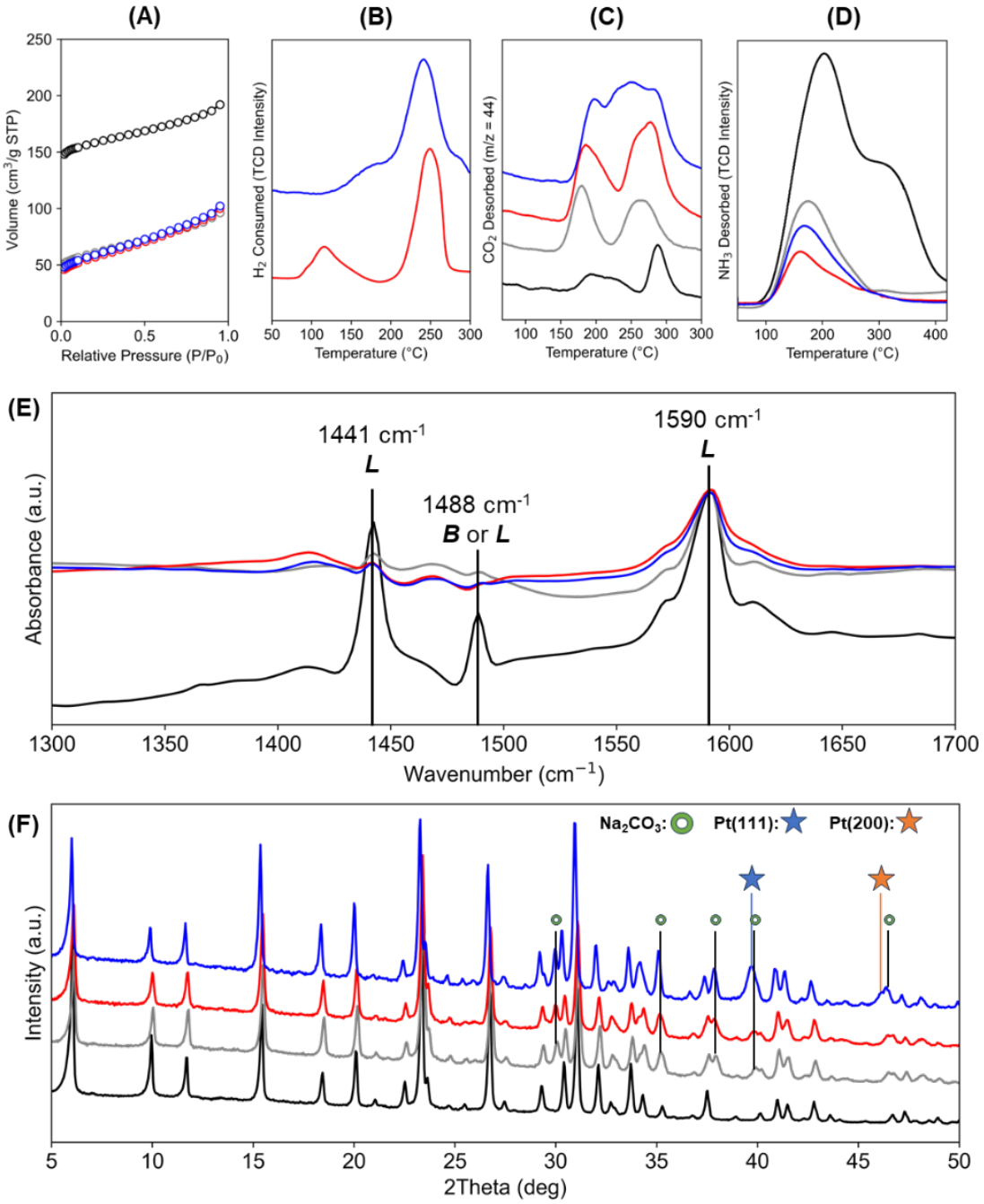

Figure 1. (A) N_2-physisorption isotherms at -196 °C following vacuum degassing at 350 °C; (B) H_2-TPR following oxidation at 400 °C (staggered for clarity); (C) CO_2-TPD following reduction at 400 °C and CO_2 saturation at 50 °C (staggered for clarity); (D) NH_3-TPD following reduction at 400 °C and NH_3 saturation at 50 °C; (E) py-DRIFTS following reduction at 400 °C, cooling to 150 °C, pyridine dosing, and N_2 purging for 120 min where B: Brønsted, L: Lewis; (F) XRD after reduction at 400 °C (staggered for clarity). Black: Na-FAU; Grey: Na/FAU; Red: Ru-Na/FAU; Blue: Pt-Na/FAU.

To test the capabilities of the ZFMs, a reactive carbon capture process was performed. In an adsorption step, the ZFM was exposed to a flow of 1,000 ppm CO_2/He for 150 min. After an inert gas purge, the catalyst was heated to 300 °C in 5% H_2/Ar (**Figure 2**A). We first evaluated Na-FAU and Na/FAU to establish the reactivity (or lack thereof) for the sorbent without transition metal active sites. Na-FAU desorbed only unreacted CO_2 (**Figure 2**B). Na/FAU (**Figure 2**C) desorbed significantly more unreacted CO_2 (centered around 150 and 300 °C) compared to Na-FAU, as expected.

Ru-Na/FAU was highly active for the conversion of captured CO_2. During the ramped temperature increase, the only carbon-containing species observed for Ru-Na/FAU was CH_4 (**Figure 2**D). Essentially no CO_2-slip (defined as the desorption of unreacted CO_2 in an RCC cycle) from the catalyst was observed during these experiments. Previous reports of Ru-based DFMs exhibited similar product distributions but were accompanied by unreacted CO_2[7]. Thus, the Ru-Na/FAU represents a benchmark material for CH_4 carbon yield (>99%) during an RCC cycle (**Table 1**). H_2O was also desorbed during the heating process, which suggested the Sabatier reaction was a likely pathway for CO_2 reduction on Ru sites. Supported Ru is known to be a high activity catalyst for the Sabatier reaction at moderate temperatures[18]. Our results are well aligned with the computational findings of Nolen et al., where the lowest energy pathway for CO_2 hydrogenation on Ru was CH_4 formation[19]. The observed selectivity was attributed to the combined facile reducibility and CO_2 affinity that allowed sequential reduction of Ru sites prior to CO_2 desorption.

Pt-Na/FAU exhibited completely different products compared to Ru-Na/FAU, forming CO (**Figure 2**E). No CH_4 was observed during the RCC cycle for Pt-Na/FAU. Between 125-200 °C, CO_2 desorbed from the Pt-Na/FAU catalyst. Above 150 °C CO began to form (along with H_2O), aligning with our expectation that CO_2 activation would only begin after Pt sites were activated.

Such high selectivity for CO over CH_4 is a notable result as Pt catalysts can promote the Sabatier or reverse water-gas shift reaction depending on support interactions[20] and reaction conditions (temperature, H_2 partial pressure)[21]. During the present RCC study, the H_2:CO_2 ratio (H_2 = 43 mbar, CO_2 = trace, Ar = 814 mbar) is much higher compared to a steady-state reaction where the intended product is CO (Equation 2, H_2:CO_2 = 1). Therefore, the Pt-Na/FAU active sites suppressed extended hydrogenation pathways (that would likely terminate in CH_4) and enabled either H-assisted or direct dissociation of CO_2 to CO. Again, combining our experimental results with computational results from Nolen et al., we postulate that CO formed via the energetically favorable H-assisted CO_2 dissociation route[19].

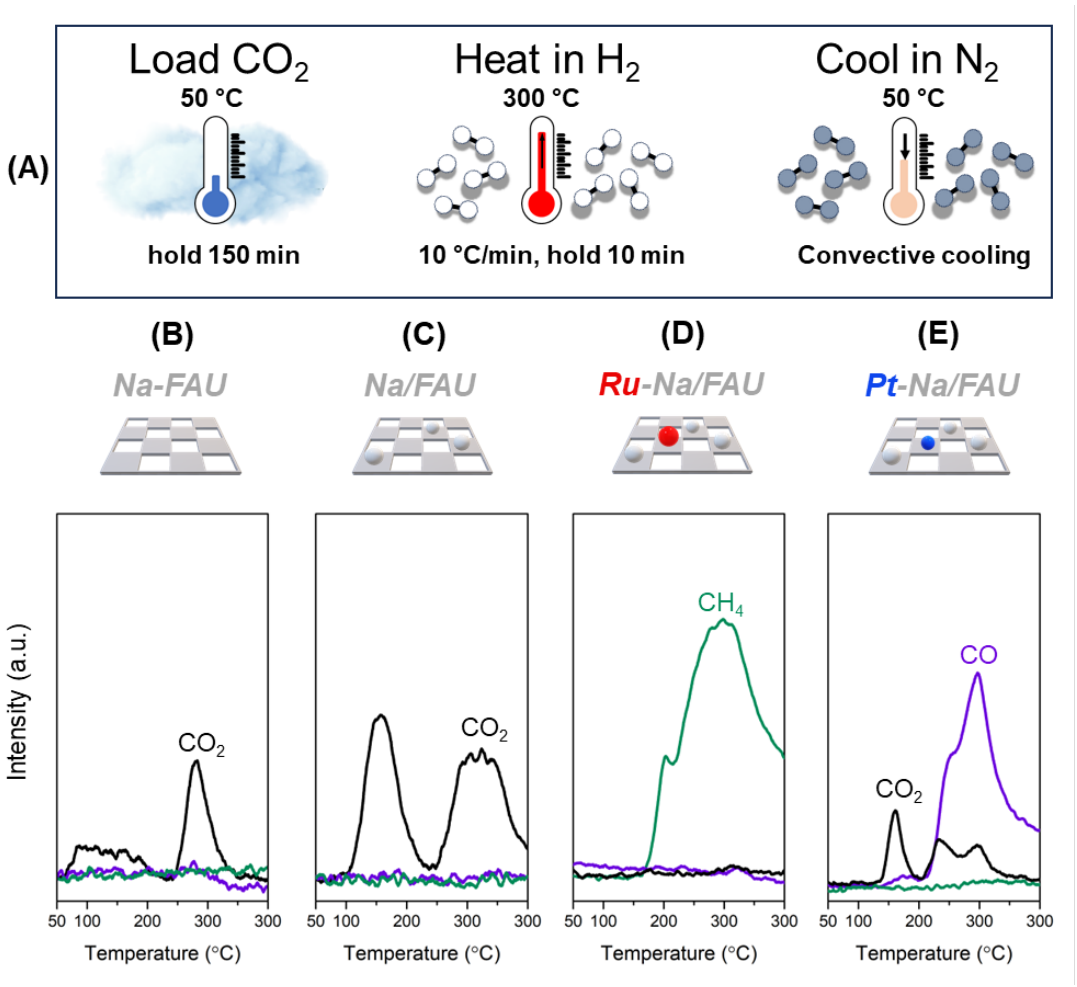

Figure 2. (A) A schematic of the employed RCC process; Gas species formed/desorbed during the RCC process on samples (B) Na-FAU, (C) Na/FAU, (D) Ru-Na/FAU, (E) Pt-Na/FAU. RCC process conditions: 1) CO_2 loading: 1,000 ppm CO_2/He, hold 150 min; 2) reduction: 5% H_2/Ar heating from 50 °C to 300 °C, hold 10 min; Cooling: N_2.

Table 1. Quantification of the products from the RCC process by integration of the MS signals.

Sample	Quantity desorbed (μmol·g^{-1})			Primary product yield (%)[a]
	CO_2	CO	CH_4	
Na-FAU	112	0	0	-
Na/FAU	275	0	0	-
Ru-Na/FAU	0	0	281	100
Pt-Na/FAU	37	175	0	83

[a]Yield = (mol product) / (mol CO_2 + mol CO + mol CH_4) * 100%

To evaluate the physical state of the Ru-Na/FAU and Pt-Na/FAU, we investigated the catalysts with scanning transmission electron microscopy (STEM) imaging and elemental dispersive spectroscopic (EDS) analysis. STEM images revealed that platinum tended to localize in discrete clusters or particles on the zeolite surfaces, whereas ruthenium spread more evenly over the support in a lacey webbing structure (**Figure S2**). Elemental composition maps indicated co-localization of Ru or Pt with Na on both ZFMs. Cation co-location has been demonstrated to increase platinum group metal redox stability[22], and to enhance catalytic activity[23]. For the ZFM catalysts, we hypothesize that the proximity of the adsorption sites and active sites promoted high activity and selectivity.

DRIFTS was implemented during a typical CO_2 RCC cycle for each catalyst to measure adsorbed surface species as products were formed (**Figure 3**). Each sample was first reduced, cooled, then exposed to 1,000 ppm CO_2/He for 30 min prior to a stepped temperature profile in 5% H_2/Ar. The presented spectra are the difference between background spectra obtained when cooling in H_2 after reduction at each respective temperature (further experimental details can be found in **Figure S3**). Spectral assignments were made by comparing the obtained spectra with literature studies of similar materials under similar conditions (**Table 2**). Evaluating the parent Na-FAU and impregnated Na/FAU samples provided sample characteristics for unreactive adsorbing/desorbing species (only CO_2 evolved from these samples on heating). Na-FAU displayed carbonate species **(Figure S4)** aligned with the anticipated bidentate (1365 and 1649 cm^{-1}) and monodentate (1429 and 1481 cm^{-1}) assignments for CO_2 adsorption on Na-FAU zeolites[24]. The splitting for the bidentate carbonate, $\Delta\nu_3$ = 284 cm^{-1}, was much greater than the splitting associated with the monodentate carbonate species, $\Delta\nu_3$ = 52 cm^{-1}, which indicated that the bidentate carbonate was less stable (and potentially more reactive)[25]. The bidentate carbonate species was associated with

a highly asymmetric, bent CO_2 molecule adsorbed to a zeolite framework O-atom (coordinated with either lattice Si or Al) and a cationic sodium atom. When Na-FAU was heated, the bidentate carbonate species was lost and the monodentate carbonate species was enhanced, matching the expectation that the monodentate carbonate is the more stable species. The monodentate species are associated with carbonates formed at Na^+ in the site III position of FAU, again matching the literature[24].

Table 2. DRIFT spectral assignments for the studied catalysts.

Species	Comment	Assignment wavenumber (cm^{-1})				Ref
		Na-FAU	Na/FAU	Ru-Na/FAU	Pt-Na/FAU	
Bidentate carbonate	Na:zeolite interface	1365	1363	1365	1365	[24,26]
Formate		n.d.	n.d.	1379	n.d.	[27,28]
Formate		n.d.	n.d.	1400	n.d.	[27,28]
Monodentate carbonate	Site III Na^+ carbonates	1429	n.d.	n.d.	n.d.	[24,26]
Monodentate carbonate	Site III Na^+ carbonates	1481	n.d.	n.d.	n.d.	[24,26]
Formate		n.d.	n.d.	1500	n.d.	[27,28]
Polydentate carbonate	"Na_2O" adsorption	n.d.	1512	n.d.	1514	[25,29]
Bidentate carbonate	Na:zeolite interface	1649	1649	1649	1649	[24,26]
Bridged-CO		n.d.	n.d.	n.d.	1898	[30]
Linear-CO		n.d.	n.d.	n.d.	2058	[30]

Not detected = n.d.

The Na/FAU sample was greatly modified from the Na-FAU sample, where essentially no monodentate carbonate species were observed at the studied temperatures and the bidentate carbonate species were enhanced. This indicated that the addition of extra-framework Na essentially eliminated CO_2 access to the site III Na^+ in the zeolite, which matched our expectations from N_2-physisorption. As access to zeolitic Na^+ appeared to be diminished in Na/FAU, the retained features at 1365 and 1649 cm^{-1} were attributed to bidentate carbonates spanning surface

$Na^{\delta+}$ ("Na_2O" sites) and zeolite framework O-atoms giving CO_2 adsorption at the Na:zeolite interface. An additional spectral feature was observed on Na/FAU at 1512 cm^{-1} and was assigned to polydentate carbonates at bulk "Na_2O" sites[25,29].

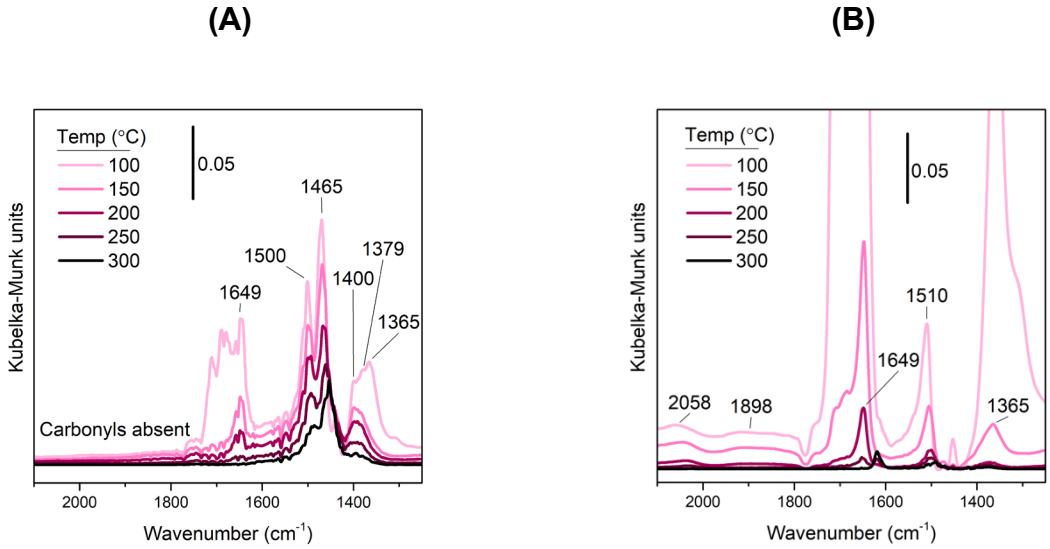

Figure 3. DRIFT spectra of an RCC cycle for the (A) Ru-Na/FAU and (B) Pt-Na/FAU catalysts. RCC process conditions: 1) CO_2 loading: 1,000 ppm CO_2/N_2 at 50 °C, hold 30 min; 2) reduction: 5% H_2/Ar heating from 50 °C to 300 °C, hold 10 min every 50 °C for data collection.

The addition of ruthenium to the catalyst promoted the evolution of gaseous CH_4 with essentially no CO_2 desorption observed when heated in H_2. The key spectral differences between Na/FAU and Ru-Na/FAU were observed in the decreased carbonate features and enhanced formate features (1379, 1400, and 1500 cm^{-1}). Formate was reported as an intermediate for CO_2 methanation over Ru/Al_2O_3[27] and Ru/TiO_2[28] catalysts where adsorbed carbonates were reduced to formate by atomic hydrogen chemisorbed on metal sites. It was also noted that formate was reactive toward the formation of adsorbed CO when it is close to the Ru metal sites[27]. This description fits well with our observations. In contrast to our findings, the previous study found that carbonyl species also formed as formate species were consumed[27,31]. Notably, the previous study was conducted at

300 °C under transient flow conditions (switching from pure CO_2 to CO_2 + H_2), whereas our study is an evaluation of pre-adsorbed CO_2 followed by heating in H_2. In a transient switching study, Marwood et al. demonstrated that the carbonyl region during CO_2 methanation on Ru/TiO_2 was sensitive to the gas composition and that at higher temperatures and higher H_2 pressures, the intensity of the carbonyl bands significantly decreased.[31] The lack of the carbonyl species on the Ru-Na/FAU system is an interesting and unexpected result that seems to indicate that CO was either not an intermediate during the present RCC cycle, or that CO had a short lifetime on the catalyst surface and was not observed while CH_4 was produced. From our interpretation of existing studies, we postulate that CO was an intermediate, but owed to the small quantity of CO_2 compared to H_2 in our system, the carbonyls were rapidly consumed to form CH_4. An additional band located at 1465 cm^{-1} was observed on the Ru-Na/FAU catalyst which did not correlate with the disappearance of other identified species and was not explicitly assigned (possible assignments include surface carbonates observed in CO methanation[32,33], CH_2 deformation observed during Fischer-Tropsch synthesis[34], or bicarbonate observed during CO_2 methanation[31]). The consumption of formate upon heating in H_2 set the Ru-Na/FAU catalyst apart from the Na/FAU and Na-FAU and indicated potential intermediates for CO_2 reduction to CH_4. Combining our findings from DRIFTS and gas-phase analysis of our RCC cycle, a reaction scheme was proposed for the reduction of captured CO_2 to CH_4 on the Ru-Na/FAU catalyst (**Figure 4**).

The Pt-Na/FAU catalyst produced CO_2 (at 100 °C) and CO (at 200 °C) when heated in H_2. CO_2 was initially desorbed without H_2O. The distinguishing features of the Pt-Na/FAU DRIFT spectra include the presence of linear (2056 cm^{-1}) and bridged carbonyls on Pt (1898 cm^{-1})[30], carbonate species, and a lack of formate species. As the catalyst was heated in H_2, carbonates were greatly reduced, and the carbonyl species were relatively consistent until 250 °C. This matches well with

the gas-phase products observed during the RCC cycle, where some CO_2 desorbed between 100-200 °C, likely unreacted carbonates. Then between 200-300 °C the product gas was primarily CO, likely owed to carbonyls species desorbing and freeing the Pt active sites for the conversion of continuously desorbing carbonate species (1365 and 1649 cm^{-1}). A potential mechanism for the Pt-Na/FAU catalysts was proposed (**Figure 4**). Thus, the Ru and Pt-Na/FAU catalysts promoted drastically different reaction pathways to form their respective products, both with outstanding selectivity.

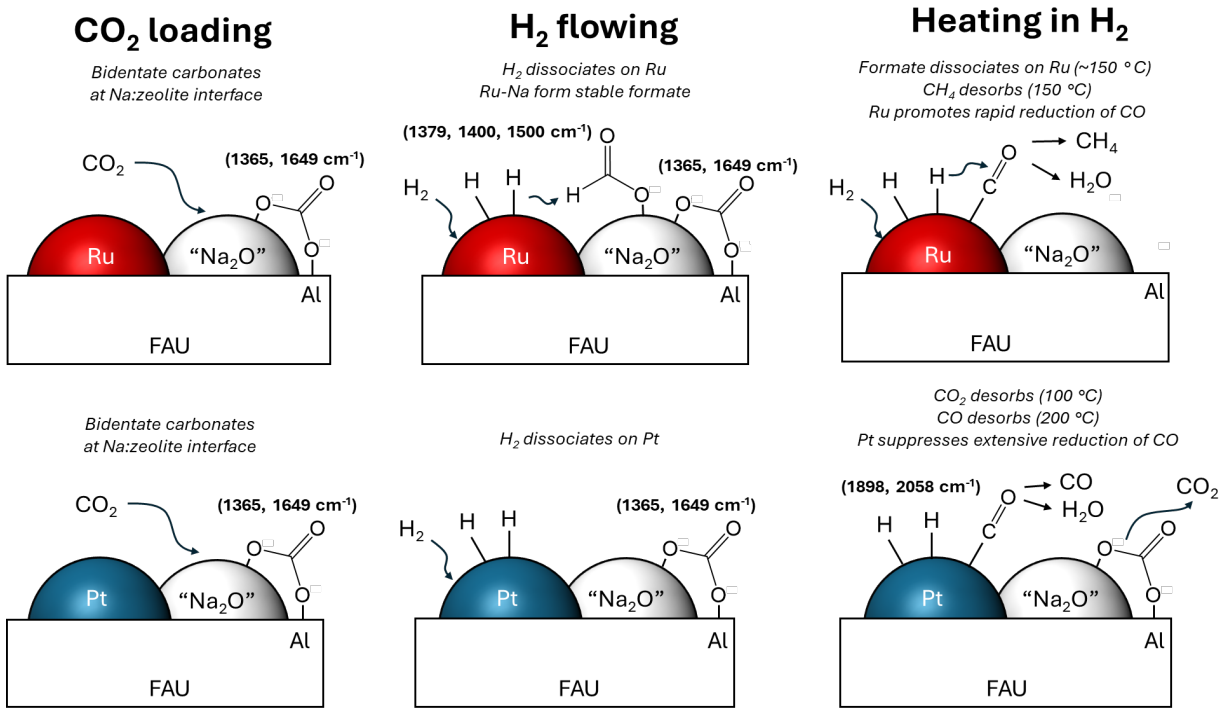

Figure 4. A proposed mechanism for the RCC process on Ru-Na/FAU and Pt-Na/FAU.

The present fundamental study reveals the process of adsorption and selective reduction of low concentration carbon dioxide over ZFMs. However, more information is required to judge the merit of these materials in the field. The first major consideration when using zeolites as hybrid sorbent-catalysts is the competition between CO_2 and H_2O adsorption. While it is generally accepted that zeolites have a strong preference for H_2O over CO_2, which would decrease their CO_2

capacity in the field, a number of recent studies have pointed out the opportunity to modify the cation exchange sites to improve CO_2/H_2O selectivity[35,36]. Another important argument for ZFMs is their use in environments with sub-ambient temperatures (<25 °C) where relative humidity is low[37]. A final argument for ZFMs would be in combination with a desiccant where atmospheric water would first be harvested from the stream for drinking water[38] or for electrolysis (to produce H_2). The dehydrated stream would then pass over the proposed materials.

Another consideration for field applicability is the presence of oxygen in the air stream. Oxygen could oxidize the reduced metal sites during CO_2 capture. We have demonstrated with TPR that our deeply oxidized Ru or Pt sites (400 °C in 10 % O_2) begin to reduce around 115°C and 175°C (in 5% H_2), respectively. Thus, we anticipate that during CO_2 adsorption in the field (near ambient temperature in ~20% O_2), the metal sites would be readily re-reduced prior to CO_2 desorption/reaction.

In closing, we have shown that ZFMs are an exciting new class of hybrid sorbent-catalysts with highly tunable CO_2 adsorption, activation, and reduction properties. Following this work, we plan to evaluate the application of zeolite dual-functional materials for higher hydrocarbon production pathways. We hypothesize that the addition of alternative catalytic active sites will change product selectivity and that modification of the alkaline oxide sorbent will modify the CO_2 uptake and desorption properties. Specifically of interest is a copper based ZFM for CO_2 to methanol upgrading using conditions recently described by Jeong-Potter et al[25]. Additionally, we are interested in evaluating the cycling stability, effect of alkali metal, and the impact of different zeolite support topologies on the overall catalytic activity of ZFMs.

AUTHOR INFORMATION

Corresponding Authors

*james.crawford4@montana.edu and matthew.yung@nrel.gov.

Author Contributions

The manuscript was written through contributions of all authors. All authors have given approval to the final version of the manuscript.

Supporting Information

Synthesis and experimental details, pyridine DRIFTS, STEM images, RCC DRIFTS, bulk chemical and physical properties of the catalyst.

Acknowledgement

The authors would like to acknowledge the financial support from the U.S. Department of Energy (DOE) Office of Fossil Energy and Carbon Management under grant FWP-FEW0277. This work was authored in part by the National Renewable Energy Laboratory, managed and operated by Alliance for Sustainable Energy, LLC, for the U.S. DOE under contract no. DE-AC36–08GO28308. Additionally, this work was supported by seed funding from the NREL Laboratory Directed Research Development (LDRD) program. Work at Lawrence Livermore National Laboratory was done under the auspices of the U.S. DOE under contract no. DE-AC52–07NA27344.

References

(1) Friedlingstein, P.; O'Sullivan, M.; Jones, M. W.; Andrew, R. M.; Gregor, L.; Hauck, J.; Le Quéré, C.; Luijkx, I. T.; Olsen, A.; Peters, G. P.; Peters, W.; Pongratz, J.; Schwingshackl, C.; Sitch, S.; Canadell, J. G.; Ciais, P.; Jackson, R. B.; Alin, S. R.; Alkama, R.; Arneth, A.; Arora, V. K.; Bates, N. R.; Becker, M.; Bellouin, N.; Bittig, H. C.; Bopp, L.; Chevallier, F.; Chini,

L. P.; Cronin, M.; Evans, W.; Falk, S.; Feely, R. A.; Gasser, T.; Gehlen, M.; Gkritzalis, T.; Gloege, L.; Grassi, G.; Gruber, N.; Gürses, Ö.; Harris, I.; Hefner, M.; Houghton, R. A.; Hurtt, G. C.; Iida, Y.; Ilyina, T.; Jain, A. K.; Jersild, A.; Kadono, K.; Kato, E.; Kennedy, D.; Klein Goldewijk, K.; Knauer, J.; Korsbakken, J. I.; Landschützer, P.; Lefèvre, N.; Lindsay, K.; Liu, J.; Liu, Z.; Marland, G.; Mayot, N.; McGrath, M. J.; Metzl, N.; Monacci, N. M.; Munro, D. R.; Nakaoka, S.-I.; Niwa, Y.; O'Brien, K.; Ono, T.; Palmer, P. I.; Pan, N.; Pierrot, D.; Pocock, K.; Poulter, B.; Resplandy, L.; Robertson, E.; Rödenbeck, C.; Rodriguez, C.; Rosan, T. M.; Schwinger, J.; Séférian, R.; Shutler, J. D.; Skjelvan, I.; Steinhoff, T.; Sun, Q.; Sutton, A. J.; Sweeney, C.; Takao, S.; Tanhua, T.; Tans, P. P.; Tian, X.; Tian, H.; Tilbrook, B.; Tsujino, H.; Tubiello, F.; van der Werf, G. R.; Walker, A. P.; Wanninkhof, R.; Whitehead, C.; Willstrand Wranne, A.; Wright, R.; Yuan, W.; Yue, C.; Yue, X.; Zaehle, S.; Zeng, J.; Zheng, B. Global Carbon Budget 2022. *Earth System Science Data* **2022**, *14* (11), 4811–4900. https://doi.org/10.5194/essd-14-4811-2022.

(2) Freyman, M. C.; Huang, Z.; Ravikumar, D.; Duoss, E. B.; Li, Y.; Baker, S. E.; Pang, S. H.; Schaidle, J. A. Reactive CO2 Capture: A Path Forward for Process Integration in Carbon Management. *Joule* **2023**, *7* (4), 631–651. https://doi.org/10.1016/j.joule.2023.03.013.

(3) Assen, N. von der; Jung, J.; Bardow, A. Life-Cycle Assessment of Carbon Dioxide Capture and Utilization: Avoiding the Pitfalls. *Energy Environ. Sci.* **2013**, *6* (9), 2721–2734. https://doi.org/10.1039/C3EE41151F.

(4) Kar, S.; Goeppert, A.; Prakash, G. K. S. Integrated CO2 Capture and Conversion to Formate and Methanol: Connecting Two Threads. *Acc. Chem. Res.* **2019**, *52* (10), 2892–2903. https://doi.org/10.1021/acs.accounts.9b00324.

(5) Duyar, M. S.; Wang, S.; Arellano-Treviño, M. A.; Farrauto, R. J. CO2 Utilization with a Novel Dual Function Material (DFM) for Capture and Catalytic Conversion to Synthetic Natural Gas: An Update. *Journal of CO2 Utilization* **2016**, *15*, 65–71. https://doi.org/10.1016/j.jcou.2016.05.003.

(6) Duyar, M. S.; Treviño, M. A. A.; Farrauto, R. J. Dual Function Materials for CO2 Capture and Conversion Using Renewable H2. *Applied Catalysis B: Environmental* **2015**, *168–169*, 370–376. https://doi.org/10.1016/j.apcatb.2014.12.025.

(7) Jeong-Potter, C.; Abdallah, M.; Sanderson, C.; Goldman, M.; Gupta, R.; Farrauto, R. Dual Function Materials (Ru+Na2O/Al2O3) for Direct Air Capture of CO2 and in Situ Catalytic Methanation: The Impact of Realistic Ambient Conditions. *Applied Catalysis B: Environmental* **2022**, *307*, 120990. https://doi.org/10.1016/j.apcatb.2021.120990.

(8) Jeong-Potter, C.; Abdallah, M.; Kota, S.; Farrauto, R. Enhancing the CO2 Adsorption Capacity of γ-Al2O3 Supported Alkali and Alkaline-Earth Metals: Impacts of Dual Function Material (DFM) Preparation Methods. *Ind. Eng. Chem. Res.* **2022**, *61* (29), 10474–10482. https://doi.org/10.1021/acs.iecr.2c00364.

(9) Arellano-Treviño, M. A.; He, Z.; Libby, M. C.; Farrauto, R. J. Catalysts and Adsorbents for CO2 Capture and Conversion with Dual Function Materials: Limitations of Ni-Containing DFMs for Flue Gas Applications. *Journal of CO2 Utilization* **2019**, *31*, 143–151. https://doi.org/10.1016/j.jcou.2019.03.009.

(10) Arellano-Treviño, M. A.; Kanani, N.; Jeong-Potter, C. W.; Farrauto, R. J. Bimetallic Catalysts for CO2 Capture and Hydrogenation at Simulated Flue Gas Conditions. *Chemical Engineering Journal* **2019**, *375*, 121953. https://doi.org/10.1016/j.cej.2019.121953.

(11) Proaño, L.; Arellano-Treviño, M. A.; Farrauto, R. J.; Figueredo, M.; Jeong-Potter, C.; Cobo, M. Mechanistic Assessment of Dual Function Materials, Composed of Ru-Ni, Na2O/Al2O3

and Pt-Ni, Na2O/Al2O3, for CO2 Capture and Methanation by in-Situ DRIFTS. *Applied Surface Science* **2020**, *533*, 147469. https://doi.org/10.1016/j.apsusc.2020.147469.
(12) Proaño, L.; Tello, E.; Arellano-Trevino, M. A.; Wang, S.; Farrauto, R. J.; Cobo, M. In-Situ DRIFTS Study of Two-Step CO2 Capture and Catalytic Methanation over Ru,"Na2O"/Al2O3 Dual Functional Material. *Applied Surface Science* **2019**, *479*, 25–30. https://doi.org/10.1016/j.apsusc.2019.01.281.
(13) Breck, D. W. Zeolite Molecular Sieves - Structure, Chemistry, and Use; John Wiley & Sons.
(14) Walton, K. S.; Abney, M. B.; Douglas LeVan, M. CO2 Adsorption in Y and X Zeolites Modified by Alkali Metal Cation Exchange. *Microporous and Mesoporous Materials* **2006**, *91* (1), 78–84. https://doi.org/10.1016/j.micromeso.2005.11.023.
(15) Tsuji, H.; Yagi, F.; Hattori, H. Basic Sites on Alkali Ion-Added Zeolite. *Chem. Lett.* **1991**, *20* (11), 1881–1884. https://doi.org/10.1246/cl.1991.1881.
(16) Zağli, E.; Falconer, J. L. Carbon Dioxide Adsorption and Methanation on Ruthenium. *Journal of Catalysis* **1981**, *69* (1), 1–8. https://doi.org/10.1016/0021-9517(81)90122-6.
(17) Ferwerda, R.; van der Maas, J. H.; Hendra, P. J. Pyridine Adsorbed on Na-Faujasite: A FT-Raman Spectroscopic Study. *J. Phys. Chem.* **1993**, *97* (28), 7331–7336. https://doi.org/10.1021/j100130a035.
(18) Crawford, J. M.; Petel, B. E.; Rasmussen, M. J.; Ludwig, T.; Miller, E. M.; Halingstad, S.; Akhade, S. A.; Pang, S. H.; Yung, M. M. Influence of Residual Chlorine on Ru/TiO2 Active Sites during CO2 Methanation. *Applied Catalysis A: General* **2023**, *663*, 119292. https://doi.org/10.1016/j.apcata.2023.119292.
(19) Nolen, M. A.; Tacey, S. A.; Kwon, S.; Farberow, C. A. Theoretical Assessments of CO2 Activation and Hydrogenation Pathways on Transition-Metal Surfaces. *Applied Surface Science* **2023**, *637*, 157873. https://doi.org/10.1016/j.apsusc.2023.157873.
(20) Kikkawa, S.; Teramura, K.; Kato, K.; Asakura, H.; Hosokawa, S.; Tanaka, T. Formation of CH4 at the Metal-Support Interface of Pt/Al2O3 During Hydrogenation of CO2: Operando XAS-DRIFTS Study. *ChemCatChem* **2022**, *14* (10), e202101723. https://doi.org/10.1002/cctc.202101723.
(21) Liu, P.; Zou, X.; Meng, X.-Y.; Peng, C.; Li, X.; Wang, Y.; Zhao, F.; Pan, Y.-X. Tuning Product Selectivity of CO2 Hydrogenation by OH Groups on Pt/γ-AlOOH and Pt/γ-Al2O3 Catalysts. *AIChE Journal* **2023**, *69* (6), e18016. https://doi.org/10.1002/aic.18016.
(22) Liu, L.; Lopez-Haro, M.; Lopes, C. W.; Li, C.; Concepcion, P.; Simonelli, L.; Calvino, J. J.; Corma, A. Regioselective Generation and Reactivity Control of Subnanometric Platinum Clusters in Zeolites for High-Temperature Catalysis. *Nat. Mater.* **2019**, *18* (8), 866–873. https://doi.org/10.1038/s41563-019-0412-6.
(23) Petrov, A. W.; Ferri, D.; Krumeich, F.; Nachtegaal, M.; van Bokhoven, J. A.; Kröcher, O. Stable Complete Methane Oxidation over Palladium Based Zeolite Catalysts. *Nat Commun* **2018**, *9* (1), 2545. https://doi.org/10.1038/s41467-018-04748-x.
(24) Jacobs, P. A.; Cauwelaert, F. H. van; Vansant, E. F. Surface Probing of Synthetic Faujasites by Adsorption of Carbon Dioxide. Part 2.—Infra-Red Study of Carbon Dioxide Adsorbed on × Zeolites Exchanged with Mono- and Bi-Valent Ions. *J. Chem. Soc., Faraday Trans. 1* **1973**, *69* (0), 2130–2139. https://doi.org/10.1039/F19736902130.
(25) Jeong-Potter, C.; A. Arellano-Treviño, M.; Wilson McNeary, W.; J. Hill, A.; A. Ruddy, D.; T. To, A. Modified Cu–Zn–Al Mixed Oxide Dual Function Materials Enable Reactive Carbon Capture to Methanol. *EES Catalysis* **2024**. https://doi.org/10.1039/D3EY00254C.

(26) Stevens, R. W. Jr.; Siriwardane, R. V.; Logan, J. In Situ Fourier Transform Infrared (FTIR) Investigation of CO2 Adsorption onto Zeolite Materials. *Energy Fuels* **2008**, *22* (5), 3070–3079. https://doi.org/10.1021/ef800209a.
(27) Wang, X.; Hong, Y.; Shi, H.; Szanyi, J. Kinetic Modeling and Transient DRIFTS–MS Studies of CO2 Methanation over Ru/Al2O3 Catalysts. *Journal of Catalysis* **2016**, *343*, 185–195. https://doi.org/10.1016/j.jcat.2016.02.001.
(28) Eckle, S.; Anfang, H.-G.; Behm, R. J. Reaction Intermediates and Side Products in the Methanation of CO and CO2 over Supported Ru Catalysts in H2-Rich Reformate Gases. *J. Phys. Chem. C* **2011**, *115* (4), 1361–1367. https://doi.org/10.1021/jp108106t.
(29) Németh, M.; Srankó, D.; Károlyi, J.; Somodi, F.; Schay, Z.; Sáfrán, G.; Sajó, I.; Horváth, A. Na-Promoted Ni/ZrO2 Dry Reforming Catalyst with High Efficiency: Details of Na2O–ZrO2–Ni Interaction Controlling Activity and Coke Formation. *Catal. Sci. Technol.* **2017**, *7* (22), 5386–5401. https://doi.org/10.1039/C7CY01011G.
(30) Serykh, A. I.; Tkachenko, O. P.; Borovkov, V. Y.; Kazansky, V. B.; Beneke, M.; Jaeger, N. I.; Schulz-Ekloff, G. Stable Subnanometre Pt Clusters in Zeolite NaX Ia Stoichiometric Carbonyl Complexes: Probing of Negative Charge by DRIFT Spectroscopy of Adsorbed CO and H2. *Phys. Chem. Chem. Phys.* **2000**, *2* (24), 5647–5652. https://doi.org/10.1039/B006609P.
(31) Marwood, M.; Doepper, R.; Renken, A. In-Situ Surface and Gas Phase Analysis for Kinetic Studies under Transient Conditions The Catalytic Hydrogenation of CO2. *Applied Catalysis A: General* **1997**, *151* (1), 223–246. https://doi.org/10.1016/S0926-860X(96)00267-0.
(32) Lorito, D.; Paredes-Nunez, A.; Mirodatos, C.; Schuurman, Y.; Meunier, F. C. Determination of Formate Decomposition Rates and Relation to Product Formation during CO Hydrogenation over Supported Cobalt. *Catalysis Today* **2016**, *259*, 192–196. https://doi.org/10.1016/j.cattod.2015.06.027.
(33) Eckle, S.; Denkwitz, Y.; Behm, R. J. Activity, Selectivity, and Adsorbed Reaction Intermediates/Reaction Side Products in the Selective Methanation of CO in Reformate Gases on Supported Ru Catalysts. *Journal of Catalysis* **2010**, *269* (2), 255–268. https://doi.org/10.1016/j.jcat.2009.10.025.
(34) Shen, J. G. C.; Ichikawa, M. Intrazeolite Anchoring of Co, Ru, and [Ru−Co] Carbonyl Clusters: Synthesis, Characterization, and Their Catalysis for CO Hydrogenation. *J. Phys. Chem. B* **1998**, *102* (29), 5602–5613. https://doi.org/10.1021/jp973038f.
(35) Fu, D.; Park, Y.; Davis, M. E. Zinc Containing Small-Pore Zeolites for Capture of Low Concentration Carbon Dioxide. *Angewandte Chemie International Edition* **2022**, *61* (5), e202112916. https://doi.org/10.1002/anie.202112916.
(36) Lee, H.; Xie, D.; Zones, S. I.; Katz, A. CO2 Desorbs Water from K-MER Zeolite under Equilibrium Control. *J. Am. Chem. Soc.* **2024**, *146* (1), 68–72. https://doi.org/10.1021/jacs.3c10834.
(37) Fu, D.; Park, Y.; Davis, M. E. Confinement Effects Facilitate Low-Concentration Carbon Dioxide Capture with Zeolites. *Proceedings of the National Academy of Sciences* **2022**, *119* (39), e2211544119. https://doi.org/10.1073/pnas.2211544119.
(38) Xu, W.; Yaghi, O. M. Metal–Organic Frameworks for Water Harvesting from Air, Anywhere, Anytime. *ACS Cent. Sci.* **2020**, *6* (8), 1348–1354. https://doi.org/10.1021/acscentsci.0c00678.